

https://dspace.org/

Optimisation of compositions and heat treatments of PT-based superalloys

Shongwe, Mxolisi Brendon

2009-10-19T10:57:56Z
http://hdl.handle.net/10539/7372

Downloaded from a DSpace repository. https://dspace.org/

Improvement of ~Pt_3Al Volume Fraction and Hardness in a Pt-Al-Ru-Cr Superalloy

M.B. Shongwe[1,2], L.A. Cornish[1,2] and R. Süss[2,3]

[1]*School of Chemical and Metallurgical Engineering, University of the Witwatersrand, South Africa*
[2]*DST/NRF Centre of Excellence in Strong Materials, University of the Witwatersrand, South Africa*
[3]*Advanced Materials Division, Mintek, Randburg, South Africa*

Abstract

Nickel-based superalloys (NBSAs) are constrained by the melting point of Ni for further increases in application temperatures, and Pt-based alloys are candidates for replacement in at least some specialised applications. Many experimental Pt-based alloys were manufactured and studied at Mintek. From the ternary alloys, the best properties were exhibited by the Pt-Al-Cr and Pt-Al-Ru samples which had ~Pt_3Al precipitates in a (Pt) matrix. However, the precipitate volume fraction was not as high as in the Ni-based superalloys. These ternary alloys were combined, and the Pt_{84}:Al_{11}:Ru_2:Cr_3 alloy was the optimum composition so far, although the volume fraction still needs improvement. Thus, this work is an attempt to increase the ~Pt_3Al volume fraction in Pt-Al-Ru-Cr alloys, by varying compositions and heat treatments.

Initially, six alloys of different compositions were selected using the optimum composition as the basis. These alloys were analysed in both the as-cast and heat treated conditions. The heat treatment comprised two stages, first at 1500°C for 18 hours and quenched in water, followed by 1100°C for 120 hours and then air cooled. Microstructural characterisation was carried out in an HR FEI Nova NanoSEM in BSE mode, also using EDX and XRD. The as-cast alloys had (Pt) dendrites with a eutectic of (Pt) + ~Pt_3Al, with tetragonal ~Pt_3Al precipitated in the dendrites. All heat treated alloys had precipitates of tetragonal ~Pt_3Al in a (Pt) matrix. The volume fraction of the precipitates varied, and the maximum proportion was 30 %. To increase the volume fraction, more samples were made with 11 at.% Al. All of the 78 at.% Pt alloys had more ~Pt_3Al precipitates than the 80 at.% Pt alloys, and the Pt_{80}:Al_{11}:Ru_5:Cr_4 alloy had no precipitates. In both conditions, most of the alloys had high hardnesses and exhibited wavy slip.

1. Introduction

The first work undertaken on PGM-based superalloys was on Rh- and Ir-based alloys [1996Yam, 1998Yam]. The rationale was that these elements not only have the fcc structure, which could permit a similar microstructure to the NBSAs, but also have higher melting points than the NBSAs – 1960°C and 2443°C for Rh and Ir respectively. Additionally, the alloys based on Rh and Ir have superior environmental resistance. Strengths reaching a maximum of 200MPa at 1800°C were obtained [1996Yam]. The high potential application temperatures of these alloys gave rise to the name "refractory superalloys" [1996Yam].

Although attractive mechanically, the simple Ir binary systems have a number of drawbacks: high density, restricted room-temperature ductility, relatively poor high-temperature oxidation resistance (Ir forms volatile oxides above 1196°C), and, most significantly, the limited physical supply of Ir in the world.

Studies of Ir-based superalloys have been extended to examine effects of alloying with Ni-based superalloys ("cross alloying") [2000Yu1, 2000Yu2]. Subsequent work involved the reduction of density and/or cost without diminishing the properties. The density was reduced by substituting some iridium in Ir_{85}:Nb_{15} with Ni, Mo, Ta, and W [2000Gu]. The best alloy was Ir_{75}:Nb_{15}:Ni_{10} (at.%), although it still had a high density compared with NBSAs and its compressive ductility was ~5% at ambient temperature [1999Gu1]. Ir-based alloys had higher strength than the Rh-based alloys, but also higher density and lower ductility [1999Gu2]. Alloys of composition $(Ir,Rh)_{75}$:Nb_{15}:Ni_{10} (at.%) were manufactured, characterised, and subjected to compression testing. All exhibited $L1_2$ precipitates and had melting temperatures above 1900°C. They had high specific strength up to 1200°C, although this decreased at higher temperatures. The best alloy, where the Ir:Rh ratio was 3:1, outperformed Ir-, Co-, and Ta-based alloys [2002Gu].

Unlike Rh and Ir, Pt enjoys relative abundance and excellent environmental resistance although it has a more modest melting point (1772°C) than Ir. A Pt solid solution can be equilibrated with an $L1_2$ phase in a number of systems [2000Wol]. The Pt-based alloys have already been successfully applied in the aerospace and glass industries [1990Lup, 1988Wha]. For these applications, exceptional chemical stability, oxidation resistance, high melting points, ductility, thermal-shock resistance, and electrical or thermal conductivity counterbalance the exceptionally high price of Pt. Pure Pt has relatively low mechanical strength; therefore, Pt is usually alloyed with up to ~20% rhodium or up to about ~30% iridium. Pt alloys with more than 20% rhodium or iridium are very difficult to process, and alloys with iridium contents of more than 20% tend to embrittle when exposed to intermediate temperatures. Pure Pt and common solid-solution Pt-rhodium alloys are highly oxidation resistant even at temperatures above 1000°C. Pt alloys show small weight losses after long exposure to high temperatures due to evaporation of the alloying element iridium. ODS Pt-based alloys are used for the most demanding applications at temperatures of up to 92% of the melting temperature of the Pt matrix [2001Fis1, 1988Wha, 1990Lup].

Following the success of the two-phase structures in iridium- and rhodium-based refractory superalloys [1996Yam, 1998Yam], a two phase microstructure in Pt-based alloys was attempted. Since Pt has the same structure as nickel and a similar chemistry, a Pt-based superalloy analogous to NBSAs was considered possible, but with a higher melting point (1769°C for Pt, compared with 1455°C for nickel) and improved oxidation resistance [1996Yam, 1997Yam, 1998Yam].

A programme was initiated at Mintek and the University of the Witwatersrand, together with other institutions to develop a range of Pt-based superalloys [2001 Hil1]. The alloys came to be based on a microstructure comprising ~Pt_3Al in a (Pt) matrix, analogous to the NBSAs. The best ternary alloys were Pt-Al-Cr and Pt-Al-Ru, and a quaternary was targetted from a combination of these alloys [2001 Hil2, 2002Cor]. Chromium stabilized the cubic $L1_2$ ~Pt_3Al precipitate, and Ru gave solid-solution strengthening to the (Pt) matrix. Experimentation gave Pt_{84}:Al_{11}:Ru_2:Cr_3 as the best composition with a reasonable proportion of precipitates (Figure 1) and good properties, including HV_{10} of 472 ± 14.

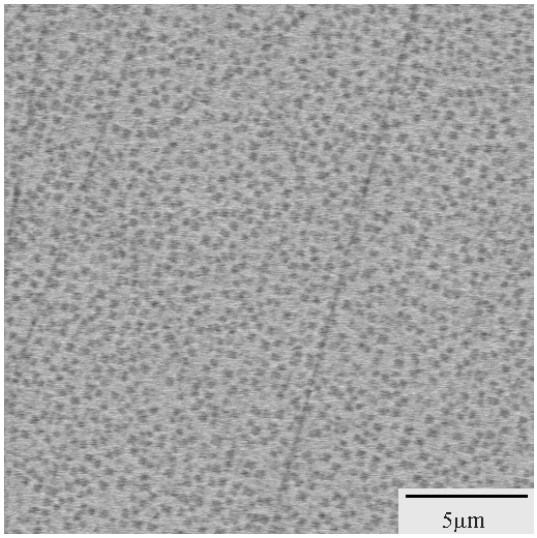


Figure 1. SEM-BSE micrograph showing Pt_{84}:Al_{11}:Ru_2:Cr_3 (at.%) with ~Pt_3Al (dark contrast) in a (Pt) matrix [2002Cor].

There were further studies to increase the precipitate volume fraction [2002Cor]. Heat treatments were conducted on the quaternary base alloys at 1150°C, 1250°C, 1350°C, and 1450°C for 96 h to verify that the microstructure could be optimised [2003Cor].

Later work at Mintek by Süss *et al.* [2006Süs], compared the Pt_{79}:Al_{11}:Cr_3:Ru_2:Co_5 and Pt_{86}:Al_{11}:Cr_3:Ru_2 alloys to increase the volume fraction ~Pt_3Al. Samples were heat treated at 1350°C and 1400°C, and cooled in three different ways: furnace cooling, air cooling and water quenching. They were examined using a High Resolution (HR) FEI Nova NanoSEM. There were reasonable volume fractions of 100-200 nm particles for furnace or air cooling from 1350°C. Furnace cooling from both temperatures also promoted the formation of ogdoadically-diced precipitates. Water quenching from either 1350°C or 1400°C yielded low volume fractions, unless the precipitates were too small to be observed.

Work has also been done at the Universities of Jena and Bayreuth, Germany. In the investigations by [2005Wen, 2004Vor], alloys with 10–13 at.% Al, 3–6 at.% Cr, 6 at.% Ni and balance Pt, showed similar two–phase microstructures to the Pt–Al–Cr–Ru alloy and lattice misfits similar to conventional NBSAs. A two–phase structure with cuboidal and $L1_2$–ordered ~Pt_3Al precipitates of about 300nm size were generated by controlled cooling after homogenization heat treatment [2004Vor] reported a ~Pt_3Al volume fraction of about 50% in an alloy with 12 at.% Al, 6 at.% Cr, 6 at.% Ni and balance Pt. The ~Pt_3Al morphology was between spherical and cuboidal. Nickel was added in various amounts as a potential solid–solution strengthener and also to lower the density and price of the Pt–based alloys [2005Wen]. The aluminum and nickel contents in the Pt–Al–Cr–Ni quaternary system were optimised to ensure a high ~Pt_3Al volume fraction and cuboidal ~Pt_3Al morphology. It was found that chromium increased the ~Pt_3Al volume fraction and decreased the absolute value of the lattice misfit between (Pt) and ~Pt_3Al. Partitioning of chromium to the (Pt) matrix phase in Pt–Al based alloys was found by several researchers [2001Hil2, 2005Wen]. The Goldsmith radius of chromium (1.25Å) is smaller than that of Pt (1.38Å) and aluminium (1.44 Å). Therefore, increasing chromium content should more strongly decrease the lattice parameter of the matrix rather than that of the ~Pt_3Al phase, and hence decrease the absolute value of the lattice misfit. A similar influence on the misfit by adding nickel (atomic radius 1.24Å) to Pt–Al–Cr–Ni alloys was also found previously by [2005Hül].

The quaternary Ir–Nb–Pt–Al system has been studied [2003Hua, 2004Hua1, 2004Hua2, 2005Hua], and an fcc/$L1_2$ two–phase structure exists in both Pt–Al and Ir–Nb binary systems and the lattice parameters of $L1_2$ phases (Ir_3Nb and Pt_3Al) are similar. However, in the Pt–Al binary system [1990Mas], two different crystal structures of Pt_3Al phase exist: the high temperature form of $L1_2$ and the low–temperature form of the distorted $L1_2$ structure DO´c. The solubility of Nb in the $L1_2$–Pt_3Al phase could not be obtained directly in the ternary alloy 86Pt–10Al–4Nb (at.%) because of the small size of the phases. Nb and Ta indicates that Nb and Ta have the similar atomic radii as Al and a similar electronic structure (being in the same group in the periodic table), which should give similar solubility characteristics. The solubility of Ta in Pt_3Al was 5 at.%; accordingly, a similar solubility is expected for Nb. No phase transformation was detected [2004Hua2, 2005Hua], which indicated that the $L1_2$–Pt_3Al structure was stabilized to room temperature in the Ir–Nb–Pt–Al system, which was attributed to Nb.

2.Experimental Procedure

Alloy buttons of mass 2g were prepared from Pt, Al, Cr and Ru of at least 99.9 % purity. The combined elements were melted in an arc-furnace in an Ar atmosphere using a Ti oxygen scavenger with a water-cooled copper hearth. Each button was turned over and re-melted at least two times to ensure thorough mixing of the elements. The alloys were named according to their nominal compositions in atomic percent. Mass losses during melting were monitored, and were found to be around 1 %. The Pt_{78}:$Al_{15.5}$:Ru_2:$Cr_{4.5}$ showed the most mass loss during melting

(1.5 %), and EDX confirmed that the alloy had the highest losses of Al, explaining the lost mass.

The as-cast alloy buttons were cut into two halves using a STRUERS automatic cutting machine and an Accutom® cutting wheel. One half of each sample was examined in the as-cast condition, while the other half was heat treated. Heat treatments were carried out in air in a Lenton muffle furnace at 1500°C for 18 hours, followed by a quench in water; then annealing at 1100°C for 120 hours and air cooling.

All samples were prepared for metallographic examination by mounting and grinding to 1200 grit on SiC paper. The samples were then polished using diamond impregnated cloths of 3µm down to 1µm followed by an oxide polishing (OP-S). In the latter, polishing is achieved through a combination of chemical treatment (the solution has a pH of 8) and gentle abrasive action, thus allowing selective polishing of the softer phases which makes etching unnecessary.

Microstructural examination of the samples was performed in a High Resolution (HR) FEI Nova NanoSEM at Mintek. The samples were imaged using backscattered electrons, and Energy Dispersive X-ray Spectroscopy (EDX) was undertaken. A working distance of 6 mm was used. The electron beam detector was set to analyze each spot area for 100 seconds. The analyses quoted are the average of at least four determinations on different areas. X-ray diffraction was used to confirm the phases identified, using Philips (PW 1710) diffractometer, with a Cu-Kα source. Spectra analysis was done using X'Pert HighScore Philips Software.

Hardness measurements on both as-cast and heat treated samples were carried out on a Vickers hard tester using a 10kg load. The analyses quoted are the average of at least five determinations on different areas. Photographs of the hardness indentions were taken using an optical microscope to obtain a qualitative evaluation of the alloys' toughness, and where visible, the slip modes.

3.Results

The samples were manufactured in two batches, the first was to ascertain the effect of Pt and aluminium content around a fairly wide spread composition, and the second was to study the effect of Cr:Ru ratios within two fixed Pt:Al contents. The microstructures of the as-cast and heat treated alloys are given in Figures 2 and 3 for both batches. Scratches can be seen on the microstructures, because sample preparation was difficult and needed longer polishing times. In all the as-cast microstructures there were dendrites of (Pt) with an interdendritic eutectic comprising (Pt) + ~Pt_3Al. In some cases, the dendrites were cored, for example in nominal samples Pt_{80}:Al_{14}:Ru_3:Cr_3 and Pt_{84}:Al_{11}:Ru_2:Cr_3 of the first batch, and especially for all the alloys of the second batch. The eutectic had a very fine structure, probably originating from both the binary eutectic and eutectoid reactions (Figure 2 and 3) and tiny cuboid precipitates were seen within the dendrites (Figure 4). In backscattered imaging, the eutectic was usually darker than the dendrites, but in the nominal Pt_{85}:Al_7:Ru_3:Cr_5 and Pt_{82}:Al_{12}:Ru_2:Cr_4 samples, the eutectic

contrast was between the contrasts of the cored dendrites. The dendrite arm spacing was estimated and is given in Table 1, together with the proportions of the eutectic, which was obtained using 10 grid placements. Image analysis was not used because the phase contrast was insufficient.

The heat treated samples showed ~Pt_3Al precipitates in a (Pt) matrix (Figure 2 and 3), although in some cases, these were difficult to discern, for example, nominal Pt_{78}:$Al_{15.5}$:Ru_2:$Cr_{4.5}$, Pt_{80}:Al_{14}:Ru_3:Cr_3 and Pt_{78}:$Al_{15.5}$:Ru_2:$Cr_{4.5}$. Some of the ~Pt_3Al precipitates were aligned in the second batch of samples, these included nominal Pt_{82}:Al_{12}:Ru_2:Cr_4 and Pt_{85}:Al_7:Ru_3:Cr_5. Also some precipitation on grain boundaries and sub-grain boundaries was seen, for example in nominal Pt_{84}:Al_{11}:Ru_2:Cr_3. The average precipitate sizes and precipitate volume fractions were derived (the latter from 10 grid placements) and are provided in Table 2.

The EDX analyses are given in Table 3. There was some loss due to evaporation on melting. The Ru and Cr mainly partitioned to the dendrites, although there was some Cr in the eutectic. The results of the hardness tests for both conditions are given in Table 4. The hardnesses quoted are the average of at least five indentations on different areas. Examples of the indentations of one alloy in both conditions are given in Figure 5, together with Pt_{80}:Al_{11}:Ru_5:Cr_4 which showed some unusual cracking and Pt_{80}:Al_{11}:Ru_6:Cr_3 which showed some pincushioning. There were also cases of barrelling. Barrelling was observed in most of the samples compared to pincushioning. Cracking around indentation is an indication of brittleness, while the slip mode around indentations shows whether the alloy has reasonable toughness by planar slip or wavy slip indicating much better resistance.

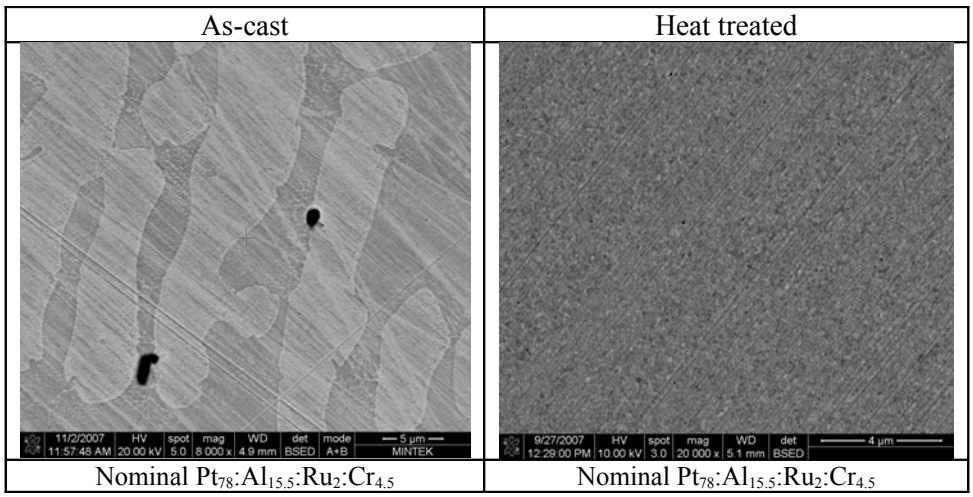


Figure 2. HR-SEM micrographs in BSE mode of the first batch of samples. As-cast samples show (Pt) dendrites (usually lighter) and the (Pt) + ~Pt_3Al eutectic. Heat treated samples show ~Pt_3Al precipitates (dark) in a (Pt) matrix (light).

Figure 2. Continued.

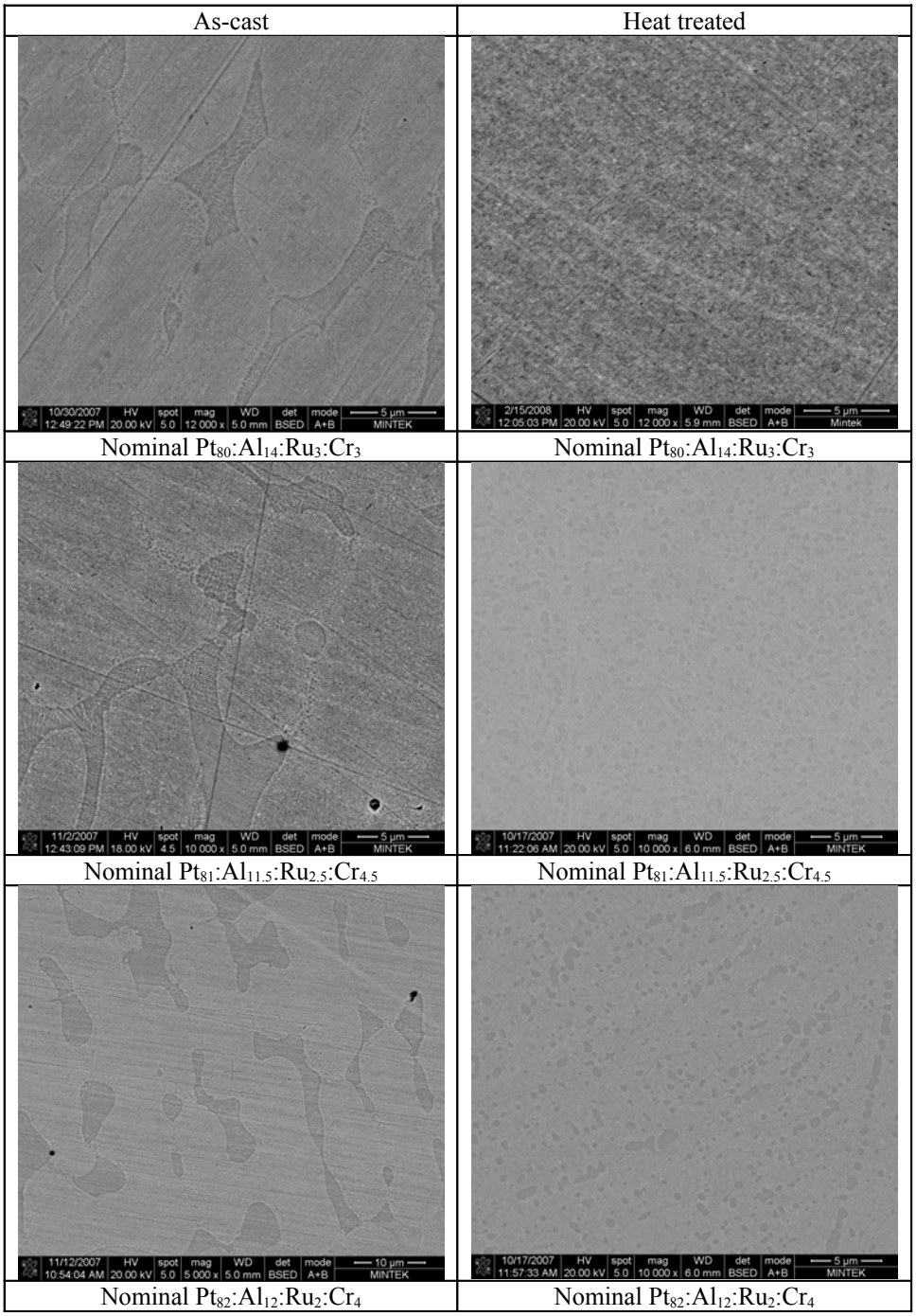


Figure 2. HR-SEM micrographs in BSE mode of the first batch of samples. As-cast samples show (Pt) dendrites (usually lighter) and the (Pt) + ~Pt_3Al eutectic. Heat treated samples show ~Pt_3Al precipitates (dark) in a (Pt) matrix (light).

Figure 2. Continued.

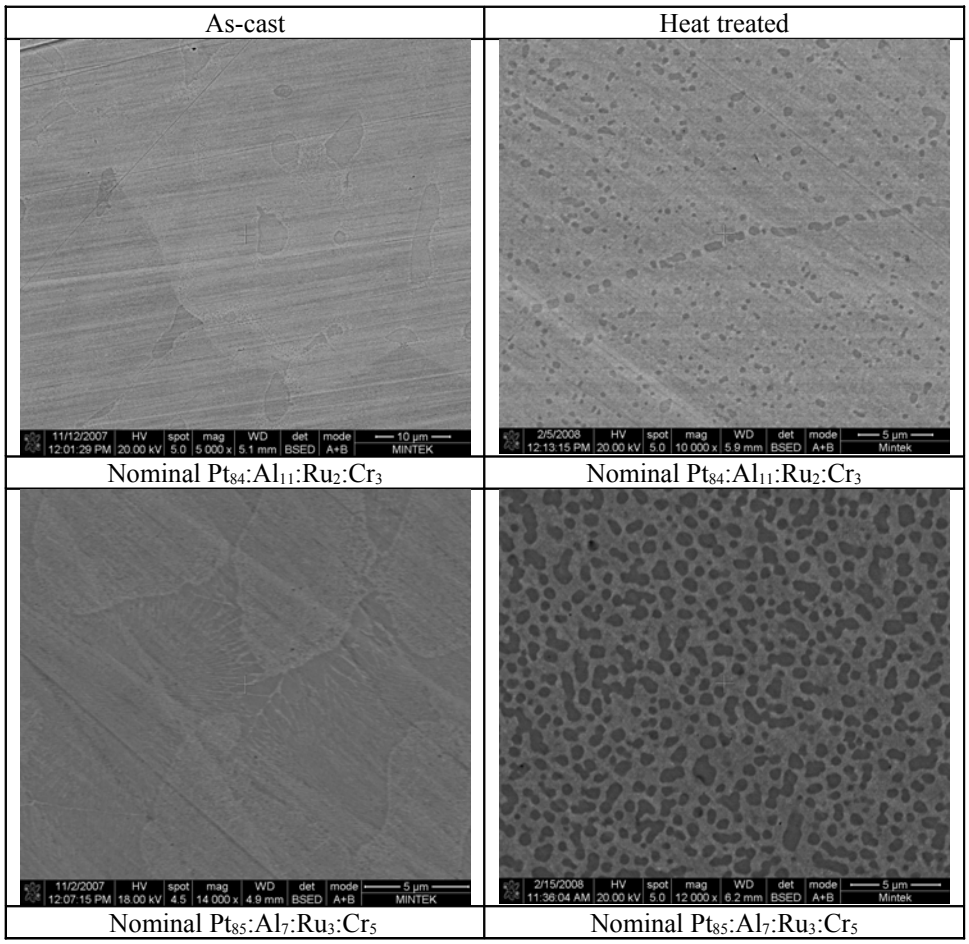


Figure 2. HR-SEM micrographs in BSE mode of the first batch of samples. As-cast samples show (Pt) dendrites (usually lighter) and the (Pt) + ~Pt_3Al eutectic. Heat treated samples show ~Pt_3Al precipitates (dark) in a (Pt) matrix (light).

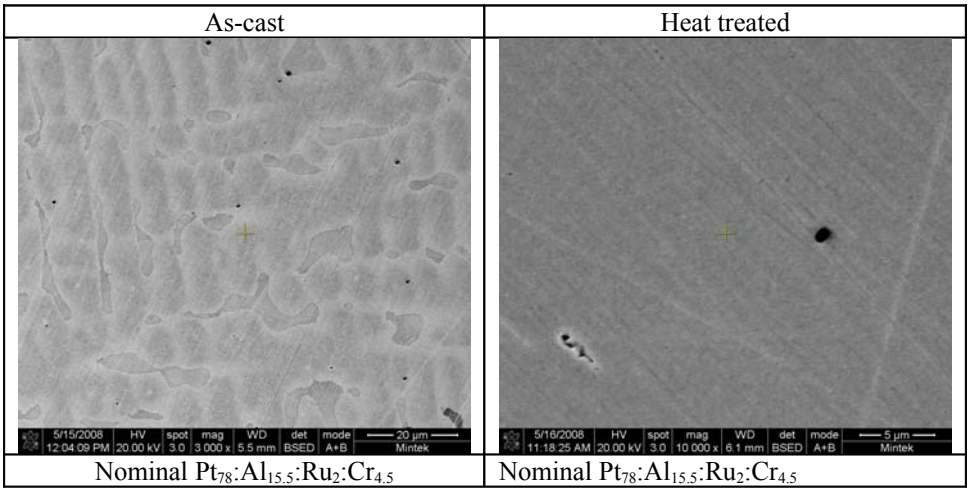


Figure 3. HR-SEM micrographs in BSE mode of the second batch of samples. As-cast samples show (Pt) dendrites (usually lighter) and the (Pt) + ~Pt_3Al eutectic. Heat treated samples show ~Pt_3Al precipitates (dark) in a (Pt) matrix (light).

Figure 3. Continued.

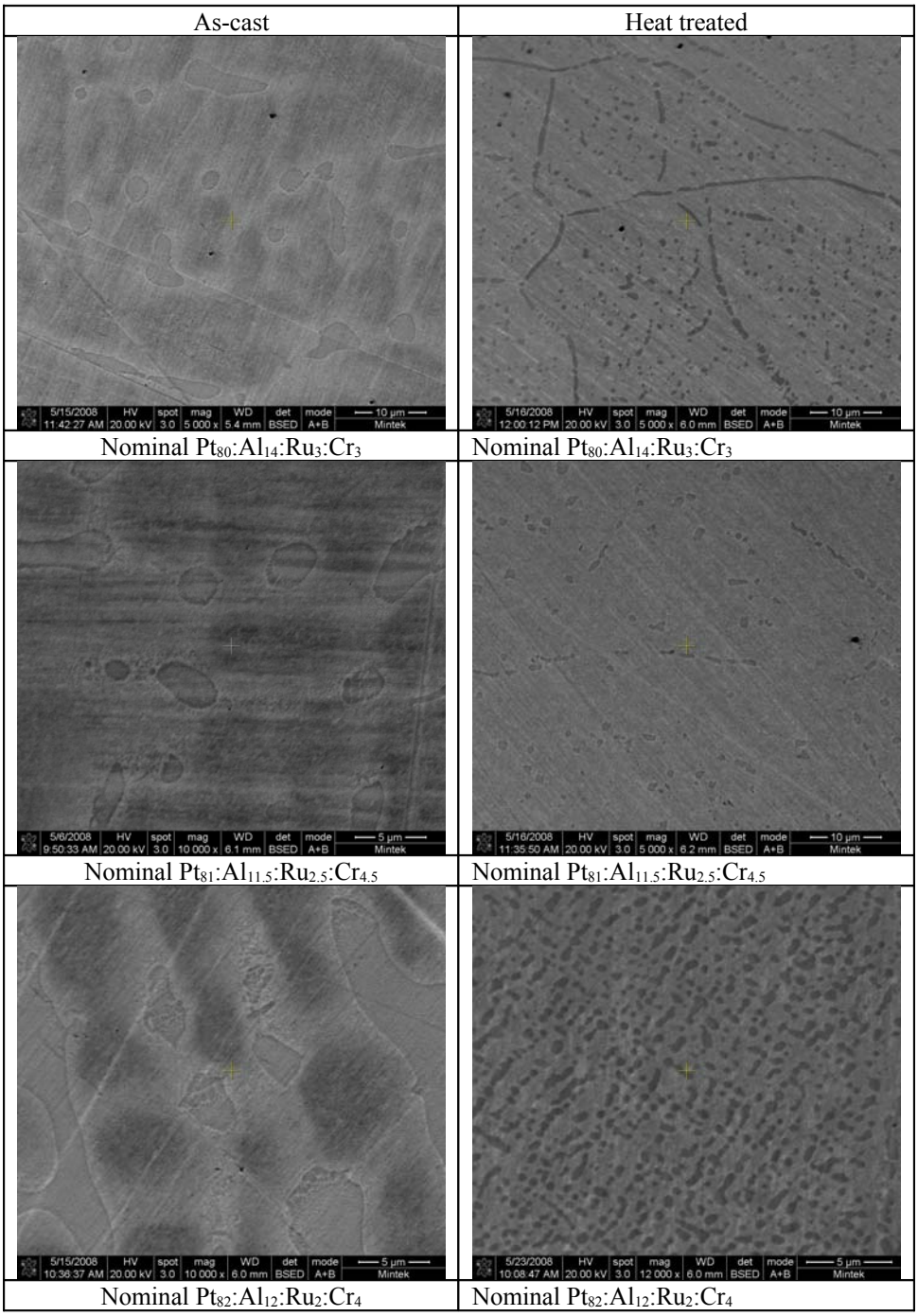


Figure 3. HR-SEM micrographs in BSE mode of the second batch of samples. As-cast samples show (Pt) dendrites (usually lighter) and the (Pt) + ~Pt_3Al eutectic. Heat treated samples show ~Pt_3Al precipitates (dark) in a (Pt) matrix (light).

Figure 3. Continued.

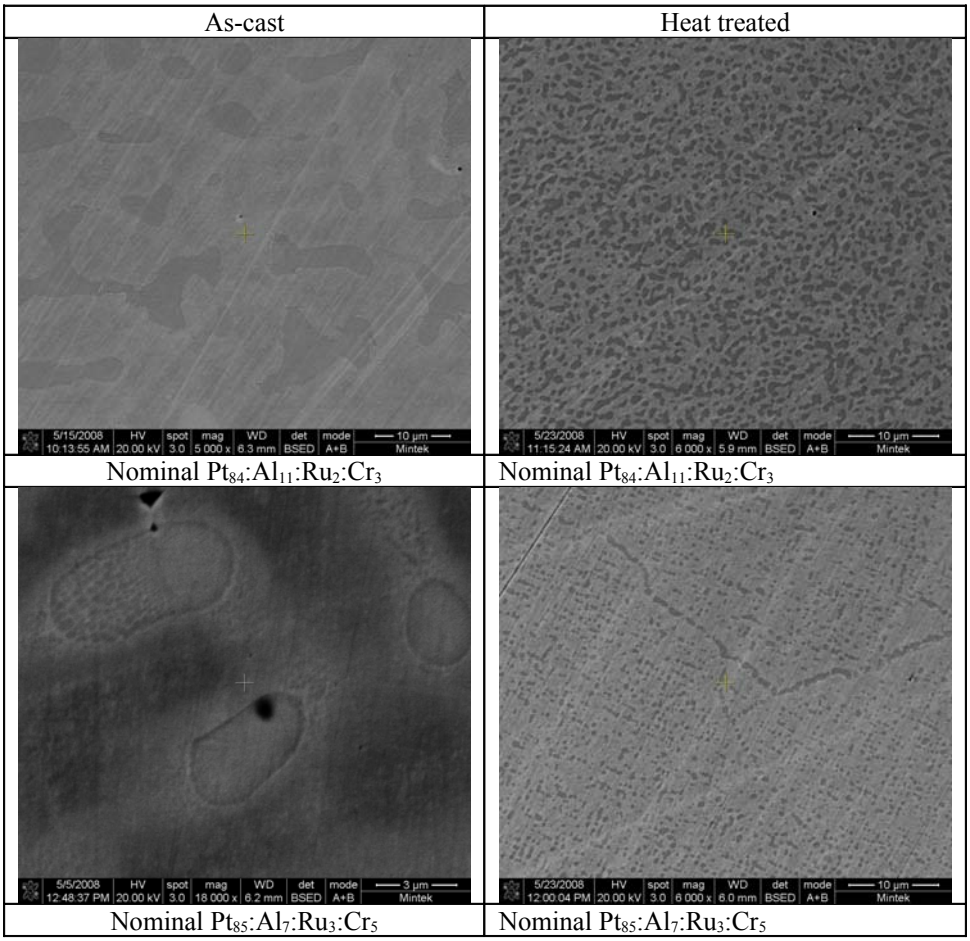


Figure 3. HR-SEM micrographs in BSE mode of the second batch of samples. As-cast samples show (Pt) dendrites (usually lighter) and the (Pt) + ~Pt_3Al eutectic. Heat treated samples show ~Pt_3Al precipitates (dark) in a (Pt) matrix (light).

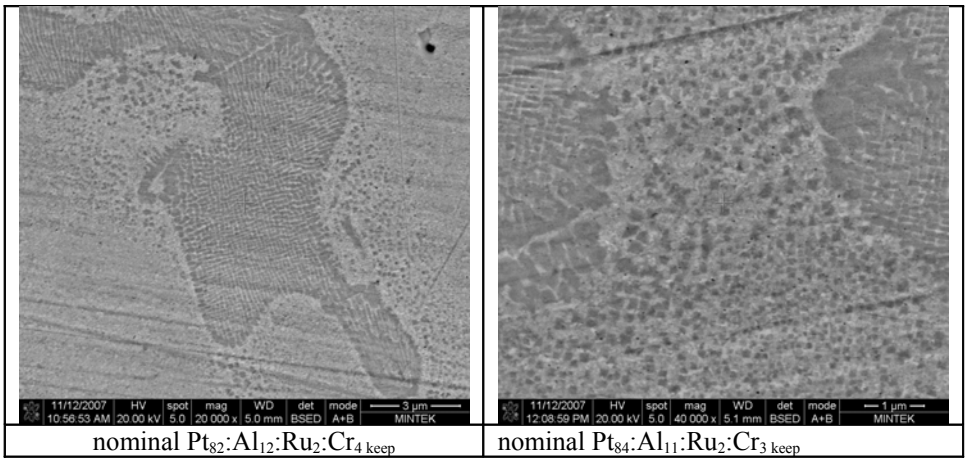
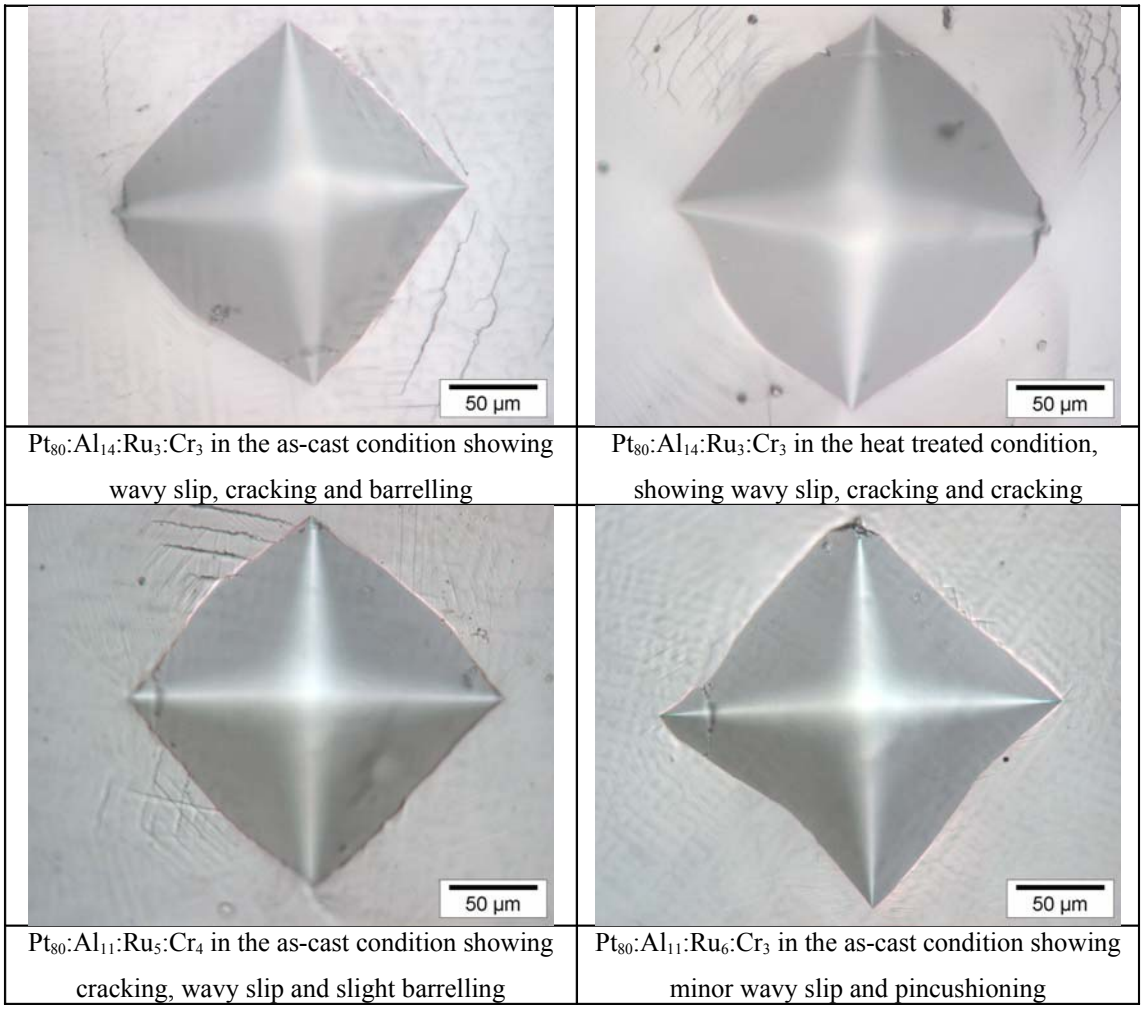


Figure 4. SEM-BSE micrographs showing the stucture of the eutectic/eutectoid and the cuboid precipitates within the dendrites.



Pt_{80}:Al_{14}:Ru_3:Cr_3 in the as-cast condition showing wavy slip, cracking and barrelling

Pt_{80}:Al_{14}:Ru_3:Cr_3 in the heat treated condition, showing wavy slip, cracking and cracking

Pt_{80}:Al_{11}:Ru_5:Cr_4 in the as-cast condition showing cracking, wavy slip and slight barrelling

Pt_{80}:Al_{11}:Ru_6:Cr_3 in the as-cast condition showing minor wavy slip and pincushioning

Figure 5. Hardness indentation micrographs for selected samples.

Table 1. Dendrite arm spacing and eutectic proportions of the as-cast samples.

Nominal Alloy (at.%)	**Average dendrite arm spacing (µm)**	**Eutectic Proportion (Fractions)**
Pt_{78}:$Al_{15.5}$:Ru_2:$Cr_{4.5}$	8.3 ± 1.5	48 ± 12
Pt_{80}:Al_{14}:Ru_3:Cr_3	5.0 ± 1.0	2 ± 1
$Pt_{81.5}$:$Al_{11.5}$:$Ru_{2.5}$:$Cr_{4.5}$	8.5 ± 1.5	16 ± 15
Pt_{82}:Al_{12}:Ru_2:Cr_4	10.7 ± 1.0	20 ± 9
Pt_{84}:Al_{11}:Ru_2:Cr_3	10 ± 1.0	7 ± 5
Pt_{85}:Al_7:Ru_3:Cr_5	8.3 ± 2.0	11 ± 6
Pt_{80}:Al_{11}:Ru_5:Cr_4	28 ± 1	8 ± 5
Pt_{80}:Al_{11}:Ru_3:Cr_6	Could not be measured	6 ± 4
Pt_{80}:Al_{11}:Ru_6:Cr_3	Could not be measured	13 ± 5
Pt_{78}:Al_{11}:Ru_5:Cr_6	9 ± 1	10 ± 10
Pt_{78}:Al_{11}:Ru_3:Cr_8	11 ± 1	6 ± 6
Pt_{78}:Al_{11}:Ru_8:Cr_3	Could not be measured	8 ± 8

Table 2. Average precipitate sizes and precipitate volume fractions of the heat treated samples.

Nominal Alloy (at.%)	Average precipitate sizes (μm)	~Pt_3Al Proportion (Fractions)
$Pt_{78}:Al_{15.5}:Ru_2:Cr_{4.5}$	Precipitates indiscernible	Precipitates indiscernible
$Pt_{80}:Al_{14}:Ru_3:Cr_3$	Precipitates indiscernible	Precipitates indiscernible
$Pt_{81.5}:Al_{11.5}:Ru_{2.5}:Cr_{4.5}$	~ 0.5	12 ± 6
$Pt_{82}:Al_{12}:Ru_2:Cr_4$	~ 0.5	10 ± 5
$Pt_{84}:Al_{11}:Ru_2:Cr_3$	~ 0.5	12 ± 5
$Pt_{85}:Al_7:Ru_3:Cr_5$	~ 1	27 ± 6
$Pt_{80}:Al_{11}:Ru_5:Cr_4$	Precipitates indiscernible	Precipitates indiscernible
$Pt_{80}:Al_{11}:Ru_3:Cr_6$	~ 1	10 ± 5
$Pt_{80}:Al_{11}:Ru_6:Cr_3$	~ 1.5	6 ± 4
$Pt_{78}:Al_{11}:Ru_5:Cr_6$	~ 0.5	24 ± 3
$Pt_{78}:Al_{11}:Ru_3:Cr_8$	~ 1.5	20 ± 3
$Pt_{78}:Al_{11}:Ru_8:Cr_3$	~ 1	10 ± 0.05

Table 3. EDX analyses of samples and phases (at.%).

Sample	Condition	Al (at.%)	Ru (at.%)	Cr (at.%)	Pt (at.%)	Phase
$Pt_{78}:Al_{15.5}:Ru_2:Cr_{4.5}$	As-cast	11.5 ± 0.7	1.7 ± 0.8	4.1 ± 0.5	82.7 ± 0.6	Overall
		19.5 ± 0.4	0.7 ± 0.0	2.2 ± 0.2	77.6 ± 0.3	(Pt) + ~Pt_3Al
		9.6 ± 0.7	1.7 ± 0.2	5.4 ± 0.3	83.3 ± 0.4	(Pt)
		12.6 ± 0.5	1.1 ± 0.3	4.5 ± 0.6	81.8 ± 0.8	(Pt) + ~Pt_3Al
	Heat treated	9.8 ± 0.7	1.5 ± 0.3	3.8 ± 0.8	84.9 ± 0.5	Overall
$Pt_{80}:Al_{14}:Ru_3:Cr_3$	As-cast	12.7 ± 0.5	2.1 ± 0.8	2.8 ± 0.8	82.4 ± 1.2	Overall
		19.2 ± 0.7	0.7 ± 0.6	1.6 ± 0.6	78.5 ± 0.3	(Pt) + ~Pt_3Al
		10.6 ± 0.8	3.2 ± 0.9	3.8 ± 0.5	82.4 ± 1.2	(Pt)
		14.5 ± 1.6	1.7 ± 0.3	1.9 ± 0.6	81.9 ± 1.9	(Pt) + ~Pt_3Al
	Heat treated	8.6 ± 0.8	2.0 ± 0.6	2.4 ± 0.9	87.0 ± 0.7	Overall
$Pt_{81.5}:Al_{11.5}:Ru_{2.5}:Cr_{4.5}$	As-cast	11.7 ± 0.3	1.7 ± 0.2	3.9 ± 0.2	82.7 ± 0.3	Overall
		20.2 ± 0.7	0.7 ± 0.3	1.4 ± 0.2	77.7 ± 0.6	(Pt) + ~Pt_3Al
		8.0 ± 1.3	2.5 ± 0.3	5.0 ± 0.4	84.5 ± 0.7	(Pt)
		13.0 ± 0.8	1.2 ± 0.2	3.1 ± 0.2	82.7 ± 0.6	(Pt) + ~Pt_3Al
	Heat treated	8.6 ± 0.5	1.4 ± 0.1	3.8 ± 0.1	86.2 ± 0.5	Overall
		21.6 ± 0.3	0.5 ± 0.3	1.6 ± 0.1	76.3 ± 0.1	~Pt_3Al
		8.5 ± 0.5	1.2 ± 0.2	3.6 ± 0.2	86.7 ± 0.2	(Pt)
$Pt_{82}:Al_{12}:Ru_2:Cr_4$	As-cast	11.2 ± 0.4	1.8 ± 0.3	3.5 ± 0.4	83.5 ± 0.6	Overall
		18.3 ± 0.1	0.6 ± 0.2	1.4 ± 0.3	79.7 ± 0.2	(Pt) + ~Pt_3Al
		10.4 ± 0.7	1.8 ± 0.1	2.5 ± 0.3	85.3 ± 0.8	(Pt)
		12.1 ± 0.3	1.1 ± 0.4	2.0 ± 0.2	84.8 ± 0.5	(Pt) + ~Pt_3Al
	Heat treated	10.3 ± 0.3	0.9 ± 0.6	3.5 ± 0.4	85.3 ± 0.5	Overall
		20.7 ± 0.4	0.5 ± 0.2	1.9 ± 0.1	76.9 ± 0.4	~Pt_3Al
		6.2 ± 0.3	2.2 ± 0.1	4.6 ± 0.2	87.0 ± 0.5	(Pt)
$Pt_{84}:Al_{11}:Ru_2:Cr_3$	As-cast	10.0 ± 0.5	1.6 ± 0.6	2.7 ± 0.2	85.9 ± 0.8	Overall
		17.9 ± 0.4	0.7 ± 0.5	1.2 ± 0.1	80.2 ± 0.6	(Pt) + ~Pt_3Al
		9.1 ± 0.5	1.4 ± 0.3	2.4 ± 0.1	87.1 ± 0.9	(Pt)
		14.2 ± 0.2	0.8 ± 0.7	1.6 ± 0.4	83.4 ± 0.5	(Pt) + ~Pt_3Al
	Heat treated	8.7 ± 0.2	1.8 ± 0.2	2.7 ± 0.4	86.8 ± 0.5	Overall
		22.1 ± 0.3	0.5 ± 0.3	1.3 ± 0.3	76.1 ± 0.5	~Pt_3Al
		7.2 ± 0.7	2.4 ± 0.2	2.7 ± 0.1	87.7 ± 0.9	(Pt)

Table 3, *Continued*. EDX analyses of samples and phases (at.%).

Sample	Condition	Al (at.%)	Ru (at.%)	Cr (at.%)	Pt (at.%)	Phase
$Pt_{85}:Al_7:Ru_3:Cr_5$	As-cast	6.1 ± 0.4	0.9 ± 0.3	3.5 ± 0.4	89.5 ± 0.6	Overall
		13.7 ± 0.1	0.6 ± 0.2	1.4 ± 0.3	84.3 ± 0.2	(Pt) + ~Pt_3Al
		2.9 ± 0.3	1.8 ± 0.4	4.9 ± 0.2	90.4 ± 0.5	(Pt)
		7.6 ± 0.7	0.8 ± 0.1	2.5 ± 0.3	89.1 ± 0.8	(Pt) + ~Pt_3Al
	Heat treated	4.1 ± 0.6	1.6 ± 0.3	4.1 ± 0.3	90.2 ± 0.3	Overall
		14.1 ± 0.2	0.7 ± 0.2	1.8 ± 0.1	83.4 ± 0.2	~Pt_3Al
		5.3 ± 0.4	1.5 ± 0.1	4.1 ± 0.1	89.1 ± 0.4	(Pt)
$Pt_{80}:Al_{11}:Ru_5:Cr_4$	As-cast	8.9 ± 0.3	4.2 ± 0.2	4.7 ± 0.5	82.2 ± 0.3	Overall
		18.2 ± 0.7	0.2 ± 0.3	1.2 ± 0.2	80.6 ± 0.6	(Pt) + ~Pt_3Al
		5.1 ± 0.8	9.9 ± 0.2	3.8 ± 0.2	81.2 ± 0.6	Cored (Pt) darker
		8.8 ± 0.8	0.7 ± 0.3	2.2 ± 0.6	88.3 ± 0.4	Cored (Pt) lighter
	Heat treated	8.9 ± 0.8	3.9 ± 0.6	3.1 ± 0.9	84.1 ± 0.7	Overall
$Pt_{80}:Al_{11}:Ru_3:Cr_6$	As-cast	8.6 ± 0.5	2.8 ± 0.8	4.1 ± 0.8	84.5 ± 1.2	Overall
		17.7 ± 0.7	0.2 ± 0.6	2.2 ± 0.6	79.9 ± 0.3	(Pt) + ~Pt_3Al
		4.6 ± 1.6	7.7 ± 0.3	1.9 ± 0.6	85.7 ± 0.8	Cored (Pt) darker
		8.1 ± 0.7	0.8 ± 0.5	5.4 ± 0.3	85.8 ± 0.6	Cored (Pt) lighter
	Heat treated	8.1 ± 0.2	2.8 ± 0.2	5.7 ± 0.4	83.4 ± 0.5	Overall
		21.6 ± 0.3	0.7 ± 0.3	2.9 ± 0.3	74.8 ± 0.5	~Pt_3Al
		9.0 ± 0.7	2.8 ± 0.2	4.1 ± 0.1	84.2 ± 0.9	(Pt)
$Pt_{80}:Al_{11}:Ru_6:Cr_3$	As-cast	7.9 ± 0.5	4.7 ± 0.6	5.8 ± 0.2	81.6 ± 0.8	Overall
		18.2 ± 0.4	0.2 ± 0.5	1.2 ± 0.3	80.6 ± 0.6	(Pt) + ~Pt_3Al
		5.2 ± 0.2	10.0 ± 0.7	2.9 ± 0.4	81.9 ± 0.5	Cored (Pt) darker
		12.0 ± 0.7	0.6 ± 0.5	3.0 ± 0.8	84.4 ± 0.3	Cored (Pt) lighter
	Heat treated	7.8 ± 0.6	4.8 ± 0.3	3.6 ± 0.3	83.8 ± 0.3	Overall
		18.9 ± 0.2	0.8 ± 0.2	2.1 ± 0.1	78.2 ± 0.2	~Pt_3Al
		7.8 ± 0.4	1.7 ± 0.1	5.1 ± 0.1	85.4 ± 0.4	(Pt)
$Pt_{78}:Al_{11}:Ru_5:Cr_6$	As-cast	9.9 ± 0.7	3.7 ± 0.8	4.4 ± 0.5	82.0 ± 0.6	Overall
		18.1 ± 0.4	0.30 ± 0.0	2.3 ± 0.2	79.4 ± 0.3	(Pt) + ~Pt_3Al
		5.1 ± 0.5	7.7 ± 0.3	4.9 ± 0.6	82.4 ± 0.8	Cored (Pt) darker
		10.4 ± 0.4	0.6 ± 0.2	5.1 ± 0.7	83.9 ± 0.4	Cored (Pt) lighter
	Heat treated	9.0 ± 0.2	3.4 ± 0.2	6.2 ± 0.4	81.4 ± 0.5	Overall
		19.9 ± 0.3	0.6 ± 0.3	2.8 ± 0.3	76.7 ± 0.5	~Pt_3Al
		8.7 ± 0.7	2.7 ± 0.2	4.2 ± 0.1	84.6 ± 0.9	(Pt)
$Pt_{78}:Al_{11}:Ru_3:Cr_8$	As-cast	9.4 ± 0.4	4.9 ± 0.3	3.1 ± 0.4	82.6 ± 0.6	Overall
		18.2 ± 0.1	0.2 ± 0.2	1.2 ± 0.3	80.6 ± 0.2	(Pt) + ~Pt_3Al
		6.2 ± 0.3	9.1 ± 0.4	3.2 ± 0.2	81.5 ± 0.5	Cored (Pt) darker
		10.9 ± 0.7	0.7 ± 0.3	3.2 ± 0.6	85.2 ± 0.4	Cored (Pt) lighter
	Heat treated	8.0 ± 0.3	2.2 ± 0.6	7.1 ± 0.4	82.5 ± 0.5	Overall
		19.7 ± 0.4	0.5 ± 0.2	2.5 ± 0.1	77.3 ± 0.4	~Pt_3Al
		7.1 ± 0.3	2.1 ± 0.1	6.0 ± 0.2	84.7 ± 0.5	(Pt)
$Pt_{78}:Al_{11}:Ru_8:Cr_3$	As-cast	9.2 ± 0.4	4.9 ± 0.3	3.1 ± 0.4	82.8 ± 0.6	Overall
		19.0 ± 0.1	0.2 ± 0.2	1.2 ± 0.3	79.8 ± 0.2	(Pt) + ~Pt_3Al
		4.4 ± 0.7	11.6 ± 0.1	3.6 ± 0.3	80.4 ± 0.8	Cored (Pt) darker
		12.7 ± 0.7	0.7 ± 0.1	2.3 ± 0.3	84.3 ± 0.8	Cored (Pt) lighter
	Heat treated	8.6 ± 0.5	4.6 ± 0.1	4.9 ± 0.1	81.9 ± 0.5	Overall
		20.5 ± 0.3	0.4 ± 0.3	1.9 ± 0.1	77.2 ± 0.1	~Pt_3Al
		10.3 ± 0.5	2.5 ± 0.2	4.8 ± 0.2	82.5 ± 0.2	(Pt)

Table 4. Hardness values (HV_{10}) and deformation modes of as-cast and heat treated samples.

	As-cast		Heat treated	
Alloy	**Hardness (HV_{10})**	**Deformation mode**	**Hardness (HV_{10})**	**Deformation mode**
$Pt_{78}:Al_{15.5}:Ru_2:Cr_{4.5}$	453 ± 26	Wavy slip	164 ± 5	Wavy slip
$Pt_{80}:Al_{14}:Ru_3:Cr_3$	390 ± 25	Wavy slip	361 ± 24	Wavy slip
$Pt_{81.5}:Al_{11.5}:Ru_{2.5}:Cr_{4.5}$	399 ± 20	Wavy slip	391 ± 24	Wavy slip
$Pt_{82}:Al_{12}:Ru_2:Cr_4$	367 ± 16	Wavy slip	378 ± 4	Wavy slip
$Pt_{84}:Al_{11}:Ru_2:Cr_3$	348 ± 53	Wavy slip	395 ± 27	Wavy slip
$Pt_{85}:Al_7:Ru_3:Cr_5$	207 ± 9	Planar slip	380 ± 17	Wavy slip
$Pt_{80}:Al_{11}:Ru_5:Cr_4$	409 ± 19	Wavy slip	247 ± 13	Planar Slip
$Pt_{80}:Al_{11}:Ru_3:Cr_6$	330 ± 30	Wavy slip	237 ± 22	Planar Slip
$Pt_{80}:Al_{11}:Ru_6:Cr_3$	383 ± 23	Wavy slip	226 ± 9	Planar Slip
$Pt_{78}:Al_{11}:Ru_5:Cr_6$	363 ± 27	Wavy slip	357 ± 4	Planar Slip
$Pt_{78}:Al_{11}:Ru_3:Cr_8$	367 ± 36	Wavy slip	354 ± 26	Planar Slip
$Pt_{78}:Al_{11}:Ru_8:Cr_3$	413 ± 18	Wavy slip	396 ± 17	Planar Slip

4.Discussion

4.1. Microstructure

The compositions of the first batch of samples were selected using the original optimum composition ($Pt_{84}:Al_{11}:Ru_2:Cr_3$) [2002Cor]. The Pt and Al contents were varied to evaluate the effect of both elements on the as-cast and heat treated samples microstructures, with Ru and Cr being kept similar for each of the samples.

All the as-cast samples were fairly homogenous as shown by the similarities of their edge and centre microstructures and compositional analyses. The proportion of the dendrites was higher than the eutectic phase and the dendrite proportion increased with increasing Pt content and decreasing Al content. Some ~Pt_3Al precipitates were observed in the dendrites, particularly close to the dendrite edges. The precipitates were coarse on the dendrite edges and finer towards the centre of the dendrites for all alloys, and the majority were rounded in shape. This was unexpected since Tshawe *et al.* [2006Tsh] observed cubic precipitates. The largest precipitates were approximately 500 nm, and the finest observed approximately 50 nm. A lighter phase within the dendrites was seen in all alloys, with its presence being more pronounced in nominal $Pt_{82}:Al_{12}:Ru_2:Cr_4$ and $Pt_{84}:Al_{11}:Ru_2:Cr_3$.

Aluminium was found to partition mostly to the interdendritic eutectic ((Pt) + ~Pt_3Al) with limited solubility in the (Pt) phase. The solubility range of Al was 13 to 22 at.% in the eutectic, and 3 to 11 at.% Al for the (Pt) dendrites. Ruthenium and Cr had limited solubility in the ((Pt) +

~Pt_3Al) eutectic, and partitioned preferentially to the (Pt). The solubility ranges were 0.5 to 0.7 at.% Ru and 1.2 to 1.7 at.% Cr for the eutectic, and between 1.4 to 3.2 at.% Ru and 2.4 to 5.4 at. % Cr for the (Pt) phase.

Similar to the as-cast samples, the heat treated samples were also fairly homogenous. Pt_{78}:$Al_{15.5}$:Ru_2:$Cr_{4.5}$ and Pt_{80}:Al_{14}:Ru_3:Cr_3 had the finest ~Pt_3Al precipitates, which were very difficult to discern in the HR-SEM. The rest of the samples (Pt_{81}:$Al_{11.5}$:$Ru_{2.5}$:$Cr_{4.5}$, Pt_{82}:Al_{12}:Ru_2:Cr_4, Pt_{84}:Al_{11}:Ru_2:Cr_3 and Pt_{85}:Al_7:Ru_3:Cr_5) had visible rounded precipitates. A lighter apparent third phase was also observed in the (Pt) matrix.

Considering the alloys' compositions, the results suggest that higher Cr contents stabilise the ~Pt_3Al phase. The average precipitate size for the samples was approximately ±1 µm. Nominal Pt_{85}:Al_7:Ru_3:Cr_5 had the highest proportion of ~Pt_3Al. For the first batch of samples, Pt_{85}:Al_7:Ru_3:Cr_5 was the most promising alloy with the highest volume fraction of ~Pt_3Al

The overall compositions for heat treated samples were different from the as-cast samples (Table 4). A marked decrease in Al was seen in all heat treated samples and was expected, since some Al could have been lost by evaporation. Aluminium was found to partition mostly to the ~Pt_3Al precipitates with limited solubility in the (Pt) phase. The solubility range of Al was 14 to 22 at.% in the precipitates, and 5 to 8.5 at.% Al in (Pt). Ruthenium had an extremely limited solubility in the ~Pt_3Al precipitates and partitioned almost exclusively to (Pt). Chromium showed solubility in both phases, but partitioned preferentially to (Pt). The solubility ranges of Ru and Cr were found to be 0.5 to 0.7 at.% Ru and 1.3 to 1.8 at.% Cr for the precipitates, while for (Pt) phase it was between 1.2 to 2.4 at.% Ru and 2.7 to 4.6 at.% Cr. The solubility of Al in ~Pt_3Al decreased with Ru and Cr additions (Figures 6 to 7).

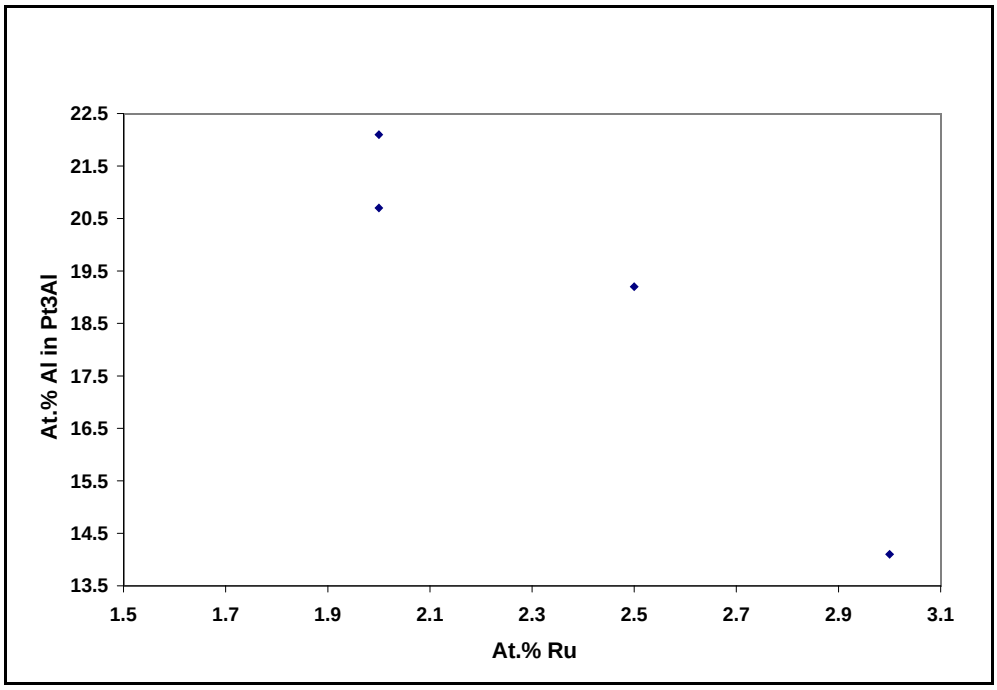


Figure 6. Solubility of Al in ~Pt_3Al with Ru additions in first batch of samples.

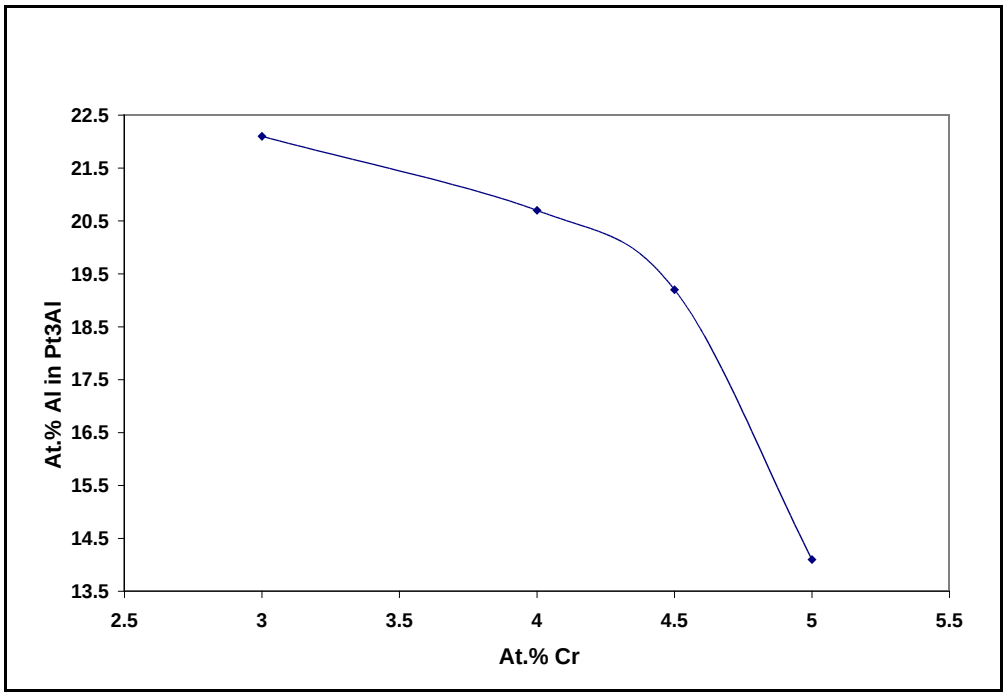


Figure 7. Solubility of Al in ~Pt_3Al with Cr additions.

For the first batch of alloys, Pt_{85}:Al_7:Ru_3:Cr_5 was found to be the most promising alloy with a high volume fraction of ~Pt_3Al precipitates and with reasonable hardness. However, the alloy had a high Pt content, which is expensive. It also had a low content of Al (7 at.%) which could allow oxidation, since Mintek's work [2000Hil, 2001Süs] has shown that about 11 at.% Al is needed to establish the thin protective oxide coating at high temperatures. Thus, in an attempt to increase the volume fraction of precipitates at low Pt content with an Al content higher than 7 at.%, a second batch of alloys was manufactured. A total of six different alloy compositions were made with 11 at.% Al, with three samples of 80 at.% Pt and another three of 78 at.% Pt, and for both sets, the Ru and Cr contents were varied. Keeping the Al content constant (for six samples) and the Pt content constant (for three samples) and varying the Ru and Cr contents would allow the effects of both elements (Ru and Cr) on the microstructure to be studied.

The second batch of the as-cast samples was similar to the first batch, although coring was more prevalent, and all samples were homogenous. In all samples, the proportion of the dendrites was higher than the eutectic phase.

The heat treated samples were fairly homogeneous and comprised ~Pt_3Al precipitates in a (Pt) matrix, except $Pt_{80}Al_{11}Ru_5Cr_4$ where the precipitates were too fine to be clearly seen, and the Pt_{80}:Al_{11}:Ru_3:Cr_6 and Pt_{80}:Al_{11}:Ru_6:Cr_3 alloys were also fairly difficult to discern. XRD confirmed the presence of tetragonal ~Pt_3Al for all samples. An apparent lighter third phase in the (Pt) matrix was observed in some samples, but was too small for reliable EDX analysis and appeared to be either contamination, or an edge effect. Sub-grains were also observed, and precipitates formed on grain boundaries and sub-grain boundaries. The morphology of the

majority of the precipitates was rounded, although a few cubic precipitates were observed in all samples. The average precipitate size was about 2 µm.

Comparison of the precipitate volume fractions shows that they increased with decreasing (Pt) content, contrary to the results obtained in the first batch of alloys. The contrary behaviour may be due to the content and ratio of Ru:Cr, since the first batch of alloys had low contents of Ru and Cr. The Cr content is high for Pt_{78}:Al_{11}:Ru_5:Cr_6, similar to the observation made in Pt_{80}:Al_{11}:Ru_3:Cr_6. Consequently, it can be noted that 6 at.% Cr is possibly the optimum required to obtain a high volume fraction of precipitates (Figure 8). A further comparison of these alloys (Pt_{78}:Al_{11}:Ru_5:Cr_6 and Pt_{80}:Al_{11}:Ru_3:Cr_6) shows that a decrease in Pt and an increase in Ru resulted in a higher volume fraction of precipitates (Figure 9). In the first batch of alloys, Pt_{85}:Al_7:Ru_3:Cr_5 had the highest volume fraction of precipitates and the Cr content is close to 6 at.% Cr. Comparing the three alloys (Pt_{78}:Al_{11}:Ru_5:Cr_6, Pt_{80}:Al_{11}:Ru_3:Cr_6 and Pt_{85}:Al_7:Ru_3:Cr_5) indicates that the optimum Ru content is possibly close to 3 at.%.

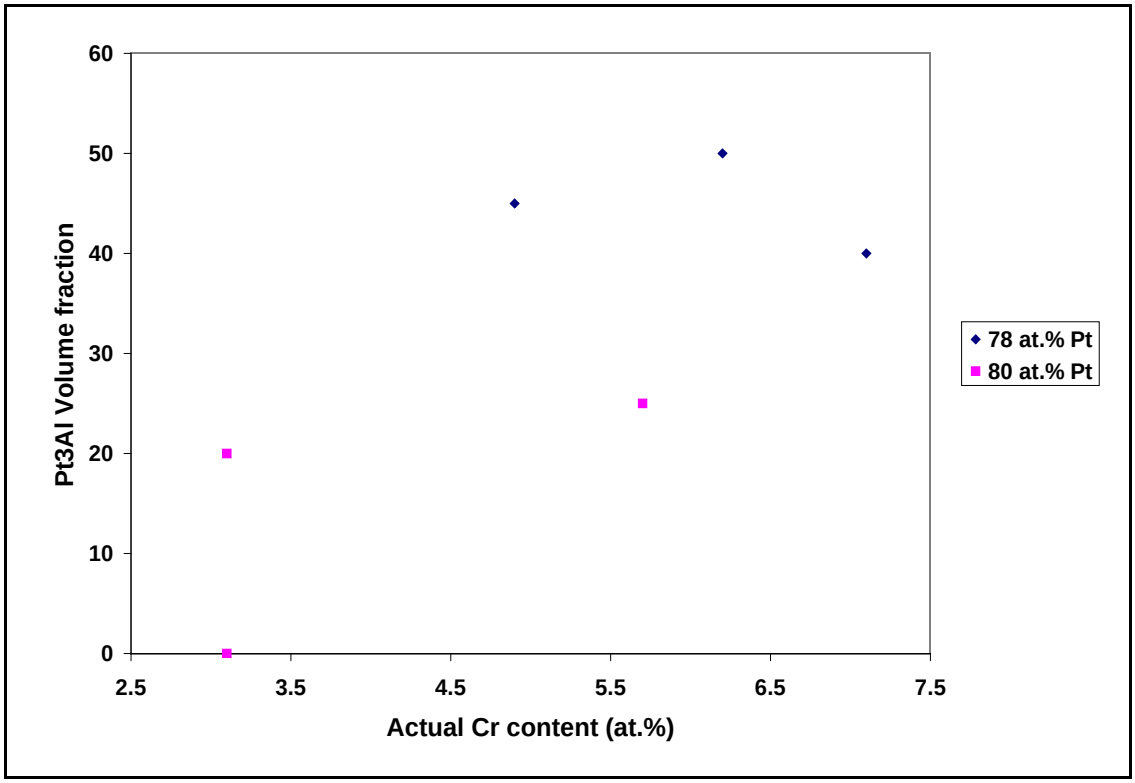


Figure 8. Relationship between ~Pt_3Al volume fraction and Cr content.

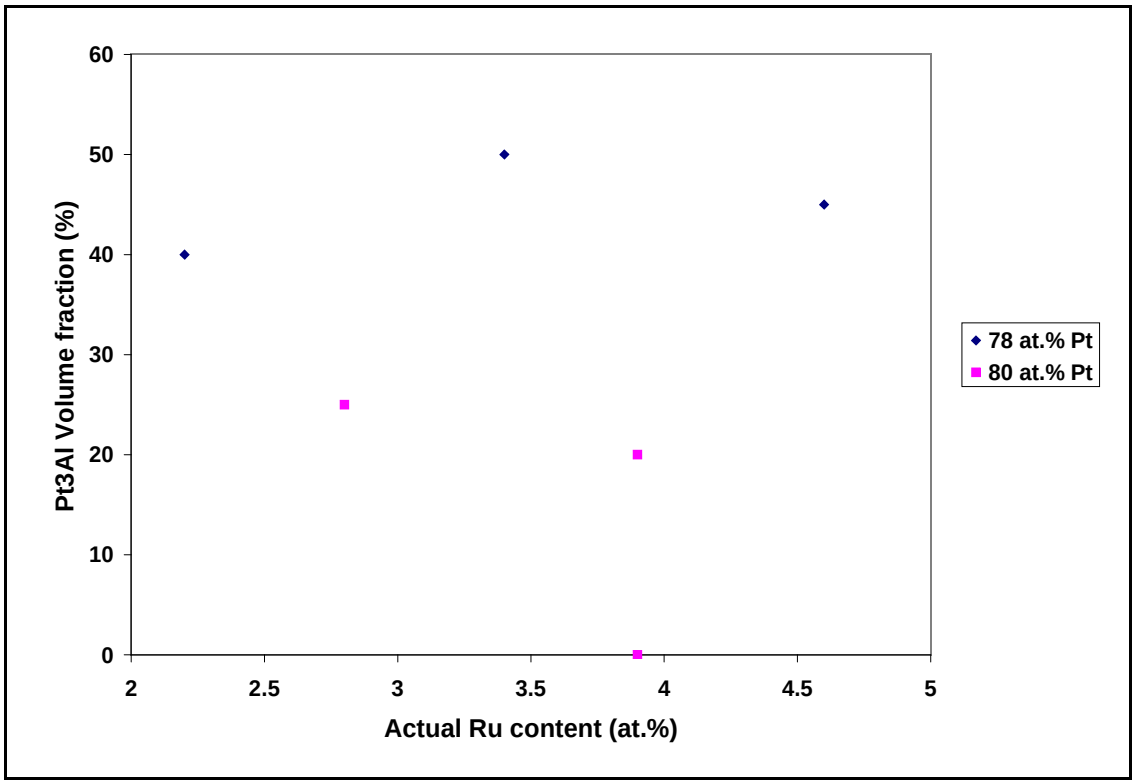


Figure 9. Relationship between ~Pt_3Al volume fraction and Cr content.

4.2. Mechanical Properties

The Pt_{85}:Al_7:Ru_3:Cr_5 alloy had a planar slip mode, which was different from the first batch of as-cast samples, probably due to its low hardness relative to the other alloys. Three of the heat treated samples (Pt_{78}:$Al_{15.5}$:Ru_2:$Cr_{4.5}$, Pt_{80}:Al_{14}:Ru_3:Cr_3 and $Pt_{81.5}$:$Al_{11.5}$:$Ru_{2.5}$:$Cr_{4.5}$) decreased in hardness compared to the as-cast samples. Pt_{78}:$Al_{15.5}$:Ru_2:$Cr_{4.5}$ had the largest decrease of about 290 HV_{10}. The other three samples (Pt_{82}:Al_{12}:Ru_2:Cr_4, Pt_{84}:Al_{11}:Ru_2:Cr_3 and Pt_{85}:Al_7:Ru_3:Cr_5) increased in hardness compared to the heat treated samples (Table 4). All samples had wavy slip. It was not possible to deduce any trend between the Pt content and the hardness of the heat treated samples.

Relating the hardness to the microstructure, heat treated alloys with higher precipitate volume fractions and coarser ~Pt_3Al precipitates ($Pt_{81.5}$:$Al_{11.5}$:$Ru_{2.5}$:$Cr_{4.5}$, Pt_{82}:Al_{12}:Ru_2:Cr_4, Pt_{84}:Al_{11}:Ru_2:Cr_3 and Pt_{85}:Al_7:Ru_3:Cr_5) had higher hardnesses than the two samples with very fine, difficult to discern precipitates. The difference between the highest hardness value and that of Pt_{85}:Al_7:Ru_3:Cr_5 was 15 HV_{10}. Thus, Pt_{85}:Al_7:Ru_3:Cr_5 had the highest precipitate volume fraction, and the highest hardness from batch 1. Pt_{85}:Al_7:Ru_3:Cr_5 also gave minor wavy slip, an indication that the alloy has better toughness.

For the second batch of samples, $Pt_{80}Al_{11}Ru_3Cr_6$ had the lowest hardness of the as-cast samples. There was no clear relationship between the Ru and Cr contents with the hardnesses of the alloys. However, it was noticed for both sets of alloys (80 and 78 at.% Pt) in the as-cast

condition that the highest hardnesses were obtained for the alloys with the lowest Cr contents (Pt_{80}:Al_{11}:Ru_5:Cr_4, Pt_{80}:Al_{11}:Ru_6:Cr_3 and Pt_{78}:Al_{11}:Ru_8:Cr_3).

All alloys in the heat treated condition had lower hardness than the as-cast samples. The 80 at.% Pt samples had lower hardness than the 78 at.% Pt samples. However, the difference in hardness of the as-cast and heat treated samples of 80 at.% Pt was less compared to the 78 at.% Pt samples. It was not possible to deduce a relationship between the Ru, Cr and hardness of the samples. The only obvious relationship was that the hardness increased with a decrease in Pt content, in contrast to what was observed in the first batch of samples. In both conditions, Pt_{78}:Al_{11}:Ru_8:Cr_3 was found to be the alloy with the highest hardness values, as well as the lowest Cr content and highest Ru content. Wavy slip was observed for all as-cast alloys, whereas all heat treated alloys gave planar slip. No relationship was deduced between the slip modes and hardnesses of the alloys.

The 78 at.% samples (with a high volume fraction of ~Pt_3Al precipitates) had higher hardnesses than the 80 at.% Pt samples. Pt_{78}:Al_{11}:Ru_5:Cr_6 has the highest hardness and precipitate volume fraction. Consequently, Pt_{78}:Al_{11}:Ru_5:Cr_6 is the most promising alloy in the second batch of samples.

For all the as-cast samples, the hardness increased with increasing eutectic content (Figure 10), although there was much scatter. An inverse relationship of hardness and dendrite arm spacing was observed (Figure 11), which is expected. Again, there was considerable scatter. For all of the heat treated samples, it was obvious that the hardness decreased with larger precipitates (~1.5μm), and the smaller precipitates gave higher hardnesses (Figure 12). The samples which had precipitates that were difficult to discern (although precipitates were present according to XRD) had either a very low hardness (~164 ± 5 for Pt_{78}:$Al_{15.5}$:Ru_2:$Cr_{4.5}$) or a relatively low hardness (361 ± 24 for Pt_{80}:Al_{14}:Ru_3:Cr_3). Considering the precipitate volumes fractions, given that ~Pt_3Al is harder than (Pt), it would be expected that higher precipitate volume fractions would give higher hardnesses. However, Figure 13 shows a peak in an overall trend of increasing hardness with increasing volume fraction.

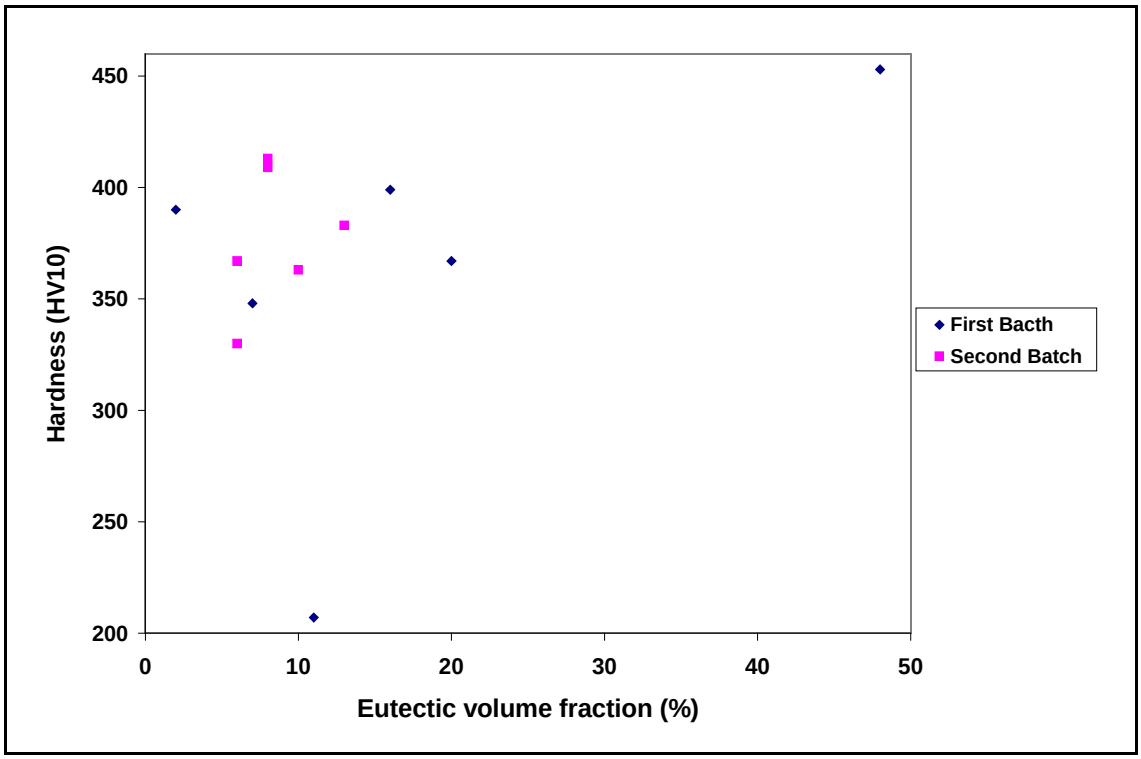


Figure 10. Relationship between hardness and eutectic volume fraction.

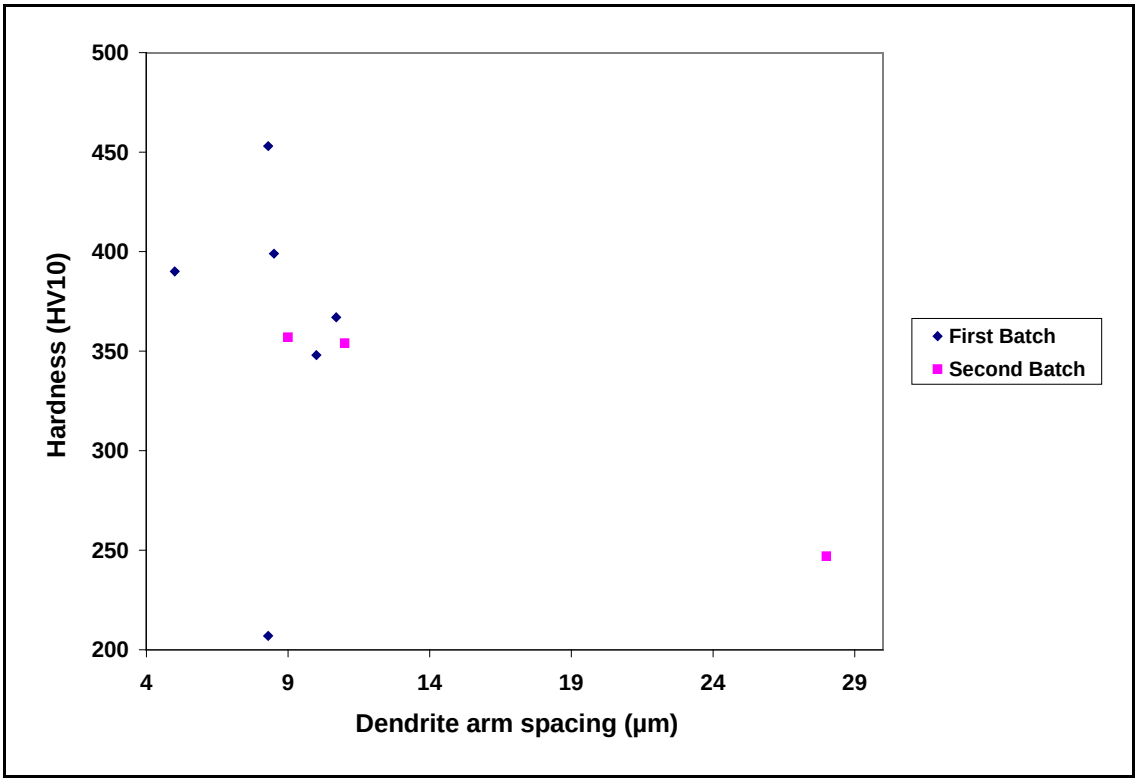


Figure 11. Relationship between hardness and dendrite arm spacing.

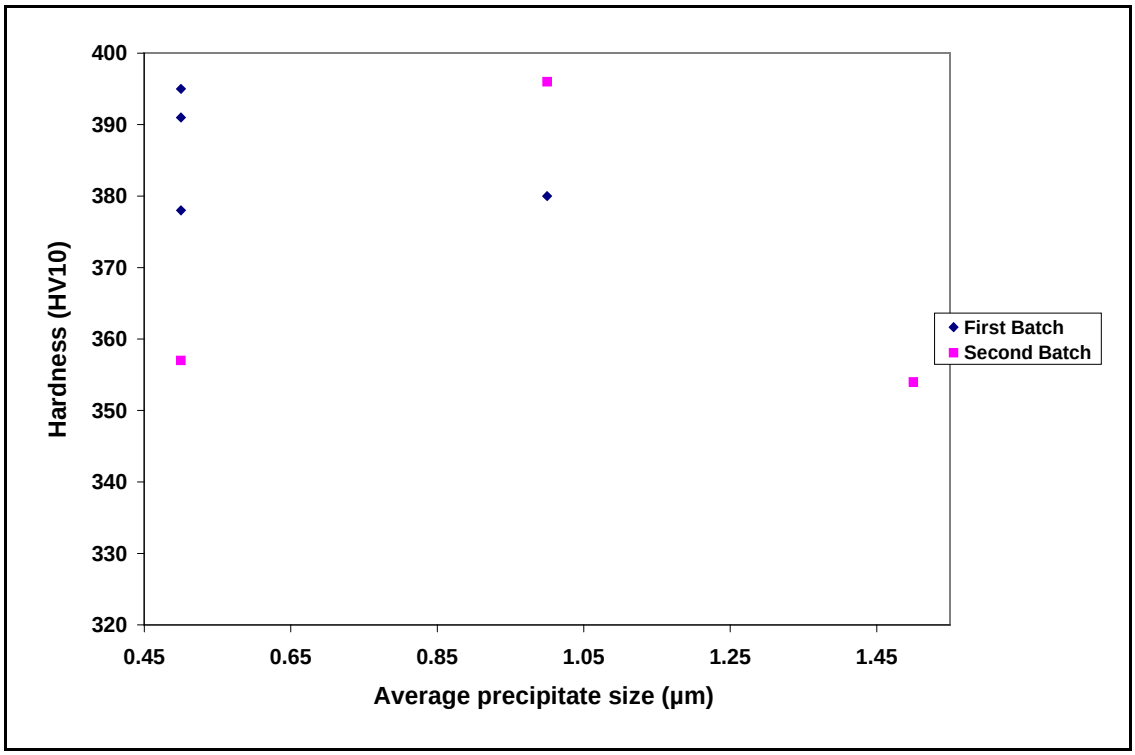


Figure 12. Relationship between hardness and precipitates size.

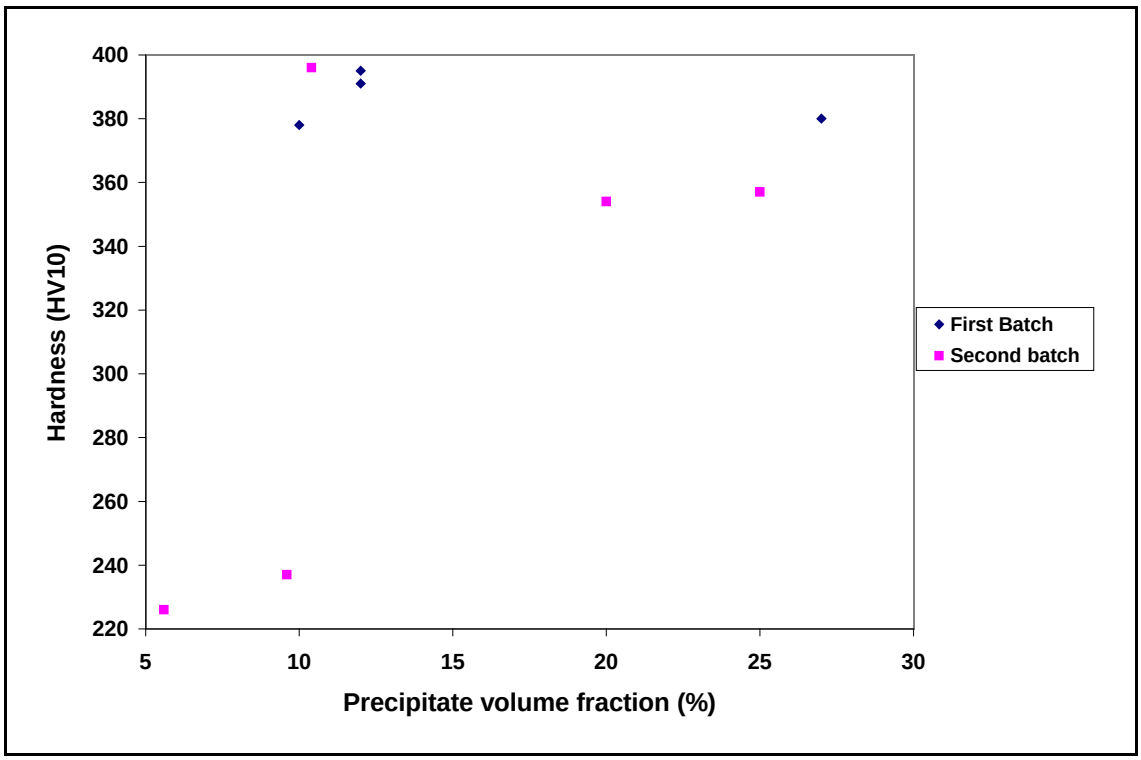


Figure 13. Relationship between hardness and precipitates volume fraction.

5.Conclusions

From the first and second batch samples, Pt_{85}:Al_7:Ru_3:Cr_5 and Pt_{78}:Al_{11}:Ru_5:Cr_6 had the highest volume fraction of ~Pt_3Al precipitates with 27 and 24 % respectively. The hardness of Pt_{85}:Al_7:Ru_3:Cr_5 was 380 ± 17 HV_{10} and 357 ± 4 for Pt_{78}:Al_{11}:Ru_5:Cr_6. From the investigations, Pt_{85}:Al_7:Ru_3:Cr_5 appears to be the optimum alloy with a high volume fraction of precipitates and reasonable hardness. However, the differences in hardnesses of Pt_{85}:Al_7:Ru_3:Cr_5 and Pt_{78}:Al_{11}:Ru_5:Cr_6 is 23 HV_{10} together with a very small difference in volume fraction of 3 % and so these alloys have similar properties. Thus, both alloys can be said to be optimum in terms of the volume fraction and hardnesses compared to the rest of the samples. From an economic viewpoint, Pt_{85}:Al_7:Ru_3:Cr_5 is unfavorable since it has a higher Pt content; and this alloy could suffer from oxidation. Thus, Pt_{78}:Al_{11}:Ru_5:Cr_6 is promising from both microstructure and economics. Further investigation will therefore be recommended on compositions close to this alloy.

Acknowledgements

This paper is published by permission of Mintek. The support of the University of the Witwatersrand, the DST/NRF Centre of Excellence in Strong Materials, Pt Development Initiative (PDI) and the Mellon Foundation are all thanked.

References

[1986Mis] Y. Mishima, Y. Oya and T. Suzuki, Proceedings of the International Conference on Martensitic Transformations, *Japan Institute of Metals*, (1986), p. 1009–1014.

[1988Wha] M.V. Whalen, *Plat. Met. Rev*., 32, 1, (1988), 2.

[1990Lup] D. Lupton, *Adv. Mater*., 5, (1990), 29.

[1990Mas] T.B. Massalski, Binary Alloy Phase Diagrams, ASM International, (1990), Ohio, USA.

[1996Yam] Y. Yamabe-Mitaria, Y. Koizumi, H. Murakami, Y. Ro, T. Maruko, and H. Haranda, *Scripta Mater*., 35 (1996), 211.

[1997Yam] Y. Yamabe-Mitarai, Y.Ro, T. Maruko, T. Yokokawa and H. Haranda, Structural Intermetallics, Proc. 2nd Int. Symp. On Structural Intermetallics, Seven Springs, Champion, U.S.A., eds. M.V. Nathal, R.Darolia, C.T. Liu, P.L. Martin, D.B. Miracle, R. Wagner and M. Yamaguchi, *Minerals, Metals & Materials Society*, 21st-26th Sept., (1997), 805-814.

[1998Yam] Y. Yamabe-Mitaria, H. Murakami, Y. Ro, T. Maruko, and H. Haranda, *Met. Mat. Trans.*, 29A (1998), 537.

[1999Gu1] Y.F. Gu, Y. Yamabe-Mitarai, Y. Ro, T. Yokokawa, and H. Haranda, *Metall. Mater. Trans. A*, 30A (1999), 2629.

[1999Gu2] Y.F. Gu, Yamabe-Mitarai, X.H. Yu, and H. Haranda, *Mater. Lett. A*, 41 (1999), 45.

[2000Gu] Y.F. Gu, Y. Yamabe-Mitarai, and H. Haranda, in Iridium, edited by E.K. Ohriner, R.D. Lanam, P. Panfilov, and H. Haranda, *Minerals, Metals and Materials Society*, Warrendale, PA, (2000), 73.

[2000Hil] P.L. Hill, P. Ellis, L.A. Cornish, M.J. Witcomb, and I.M. Wolff, Proc. High-Temperature Corrosion and Protection 2000, Sapora, Japan, 17nd-22nd Sept, (2000), 185-190.

[2000Wol] I.M. Wolff, and P.J. Hill, *Plat. Met. Rev.*, (2000), 44, (4), 158-166.

[2000Yu1] X.H. Yu, Y. Yamabe-Mitarai, Y. Ro, and H. Haranda, *Met. Mat. Trans.*, (2000), 31A, 173.

[2000Yu2] X.H. Yu, Y. Yamabe-Mitarai, Y. Ro, and H. Haranda, *Key Engineering Materials*, Vols. 171-174, (2000), 677-684.

[2001Fis1] B. Fischer, D. Freund, J. Merker, R. Völkl, and D.F. Lupton, in Proc. 8th Int. Conf. on Composites Engineering, edited by D. Hui, University of New Orleans, New Orleans, LA, (2001), 249.

[2001Hil1] P.J. Hill, T. Biggs, P. Ellis, U. Hohls, S. Tailor, and I.M. Wolff, *Mat. Sci. Eng*., A301, (2001), 167

[2001Hil2] P.J. Hill, L.A. Cornish, P. Ellis, and M.J. Witcomb, *J. Alloys & Compounds*. 322, (2001), 166.

[2001Süs] R. Süss, P.J. Hill, P. Ellis and I.M. Wolff, Proc. 7th European Conference on Advanced Materials and Processes, Rimini, Italy, 2001.

[2002Cor] L.A. Cornish, J. Hohls, P.J. Hill, S. Prins, R. Süss and D. Compton, *J. Mining & Metallurgy*, 38 (3 – 4) (2002), 197 – 204.

[2002Hil] P.J Hill, N. Adams, T. Biggs, P. Ellis, S. Taylor, and I.M. Wolff, *Mat. Sci. Eng., A*, 338 (2002), 133-141.

[2002Gu] Y.F. Gu, Y. Yamabe-Mitarai, S. Nakazawa, Y. Ro, and H. Haranda, *Met. Mat. Trans*. 33A, (2002), 1281-1283.

[2003Hua] C. Huang, Y. Yamabe-Mitarai, K. Nishida and H. Harada. *Intermetallics*, 11, (2003), 917–926.

[2004Hua1] C. Huang, Y. Yamabe–Mitarai and H. Harada, *J. Alloys & Compounds*, 366 (2004), 217–221.

[2004Hua2] C. Huang, Y. Yamabe-Mitarai, S. Nakazawa and H. Harada. *Mater. Lett.*, 58, (2004), 483–488.

[2004Vor] S. Vorberg, M. Wenderoth, B. Fischer, U. Glatzel, and R. Völkl. *JOM*, 56(9), (2004), 40–43.

[2005Hua] C. Huang, Y. Yamabe-Mitarai, X.H. Yu, S. Nakazawa and H. Harada. *Met. & Mat. Trans.*, vol. 36A, (2005), 539–545.

[2005Hül] M. Hüller, M. Wenderoth, S. Vorberg, B. Fischer, U. Glatzel, and R. Völkl, *Met. Mat. Trans.*, 36A, 3A,(2005), 681-689.

[2005Wen] M. Wenderoth, L.A. Cornish, R. Süss, S. Vorberg, B. Fischer, U. Glatzel and R. Völkl. *Met. & Mat. Trans.*, vol. 36A, (2005), 567–575.

[2006Süs] R. Süss and L.A. Cornish. Unpublished Mintek Work (2006).

[2006Tsh] W. Tshawe, A. Douglas, B. Joja and L.A. Cornish, Proc. Microsc. Soc. south Afr., Volume 36, p. 15, Port Elizabeth, 28th November – 1st December 2006.